Response of FSSP-100 and PVM-100A to Small Ice Crystals

H. GERBER

Gerber Scientific, Inc., Reston, Virginia

P. J. DEMOTT

Colorado State University, Fort Collins, Colorado

(Manuscript received 31 October 2013, in final form 13 February 2014)

ABSTRACT

Correction factors C_f are derived for ice-crystal volume and effective radius Re, measured by Forward Scattering Spectrometer Probe (FSSP) and Particulate Volume Monitor (PVM) that are known to overestimate both parameters for nonspherical particles. Correction factors are based on ice-crystal volume and the projected area of randomly oriented model ice crystals with column, rosette, capped-column, and dendrite habits described by Takano and Liou. In addition, C_f are calculated for oblate and prolate spheroids. To test C_f, both probes are compared to small, predominately solid hexagonal ice-crystal plates and columns generated in the Colorado State University (CSU) Dynamic Cloud Chamber (DCC). The tendency of heat released by the PVM (placed inside the chamber) to evaporate ice crystals and the smaller upper size range of the PVM than the size range of the FSSP caused large differences in the probes' outputs for most comparisons in the DCC. Correction factors improved the accuracy of Re measured by the FSSP for the solid hexagonal crystals, and both probes produced similar results for the projected area and ice water content when crystal sizes fell within the probes' size ranges. The modification for minimizing ice-crystal shattering and the application of C_f for forward scatter probes such as the FSSP suggests the probes' improved usefulness for measuring small ambient ice crystals.

1. Introduction

The size of ice crystals in atmospheric cirrus clouds can have strong vertical dependence in cirrus clouds with the smallest crystals near cloud top, as illustrated by Heymsfield and Miloshevich (2003). Heymsfield et al. (2010) also show that ice crystals smaller than 50-μm diameter can contribute substantially to total ice water content IWC of cirrus clouds, especially at lower temperatures and for IWC $< 0.1\,\mathrm{g\,m^{-3}}$. It thus is important to measure the contribution of the smaller ice crystals to IWC as well as other properties, such as their effective radius Re. Aircraft instrumentation designed to measure individual spherical particles less than ~50-μm diameter include the Cloud Droplet Probe (CDP) and Cloud and Aerosol Spectrometer (CAS), both from Droplet Measurement Technologies; the Forward Scattering Spectrometer Probe (FSSP) formerly from Particle Measuring Systems, Inc.; and the Particulate Volume Monitor (PVM) from Gerber Scientific, Inc. These instruments (particle spectrometers except for the last one) measure light scattered in the near-forward direction by individual particles irradiated by a narrow beam of light. The scattered light is related to the size and concentration of the particles to yield spectra that are integrated to provide information on the bulk properties of the particles, such as particle volume and surface area. The PVM produces directly estimates of total particle volume and total particle surface area PSA of spherical particles.

The listed instruments should be able to measure accurately near-spherical ice crystals within their size range, which has been borne out by practice (see, e.g., Gerber et al. 1998; Young et al. 1998; Gayet et al. 1996, 2012). However, for aspheric crystals such as plates, columns, and more complex shapes, questions remain on how to interpret the output of the instruments. A recent review of airborne instruments suggests that probes such as the FSSP and PVM are suitable only when the liquid phase is present (Baumgardner et al. 2011), and a current book (Wendisch and Brenguier 2013) detailing airborne

Corresponding author address: Hermann Gerber, Gerber Scientific, Inc., 1643 Bentana Way, Reston, VA 20190.
E-mail: hgerber6@comcast.net

DOI: 10.1175/JTECH-D-13-00228.1

measurement techniques notes that caution must be used in interpreting particle-scattering measurements in ice- and mixed-phase clouds.

Part of the uncertainty with these instruments has been the shattering of large crystals on the instruments' inlets, causing spurious ice-crystal sizes and concentrations, which Gardiner and Hallett (1985) had originally suggested for the FSSP; see also McFarquhar et al. (2007), Heymsfield (2007), Jensen et al. (2009), and Korolev et al. (2011, 2013). The Korolev references describe modifications to the leading edges of the instruments that reduce the shattering effect, suggesting that these instruments now may be more useful for measuring small ice crystals.

Some modeling attempts have been made to determine the response of single-particle spectrometers to small ice crystals. Borrmann et al. (2000) calculated the response of the FSSP-300 for rotationally symmetrical ellipsoids with maximum axes less than $\sim 20\,\mu$m in length and found good agreement with Mie theory. Febvre et al. (2012) found that the agreement between small hexagonal plates and columns and Mie theory depended on the assumed roughness of the crystal faces.

The purpose of the present study is to evaluate the response of the FSSP-100 and PVM-100A for small ice crystals. An observational study held earlier (Gerber et al. 1995, hereinafter G95) at the Colorado State University (CSU) Dynamic Cloud Chamber (DCC) provides the data for the present evaluation. Small ice crystals consisting of plates, columns, plates with some dendritic structure, and quasi spheres were generated in the DCC and observed with the FSSP-100, PVM-100A, 230-X (1D spectrometer), and with a video microscope for characterizing the shapes and sizes of the crystals. The FSSP and PVM observations are compared to each other, and correction factors are applied to the observations using the Takano and Liou (1995) calculations for the geometric cross-sectional area (also termed projected area) of randomly oriented crystals with crystal habits similar to those generated in the DCC.

The following describes the DCC, the optical characteristics of the FSSP and PVM, the derivation of the correction factors, the measurements in the DCC, and our results and conclusions.

2. Instrumentation

a. DCC

The following summarizes the main features of the DCC described and used previously (DeMott 1988, 1990; DeMott and Rogers 1990), and for the present study (G95). The DCC consists of a 2-m^3 pressure vessel encasing a 1.2-m^3 thermally controlled copper cloud chamber that can be cooled to match adiabatic cooling during expansion, and with vents and windows for probes and aerosol and gas injection. The range of operation of the chamber for temperature is from +40° to −55°C for temperature, from 90 to 50 kPa for pressure, from 0.1% to >100% for relative humidity RH, and from 0.2 to 20 m s^{-1} for simulated vertical velocity.

Thermocouples measure the inside wall and air temperatures, and dewpoint hygrometers are used to measure RH. A condensation nucleus counter measures ice and condensation nuclei.

The video microscope consists of a continuously moving loop of 16-mm film exposed to sedimenting ice crystals at the base of the inner (cloud) chamber of the DCC. The film exits the chamber and passes by a charge-coupled device (CCD) camera with a microscopic zoom lens, and the CCD images then pass to a video recorder. Manual evaluation of the crystal images provides information on crystal sizes and shapes.

The FSSP draws air horizontally out of the chamber with a converging horn in which the air is accelerated to $\sim$28 m s^{-1} (DeMott and Rogers 1990). Potential and undocumented uncertainties in the FSSP measurements include crystal trajectories that deviate from the streamlines in the horn and crystal impaction on the inner surface of the horn. Air for the 1D draws air vertically out of the chamber. The PVM is situated near the bottom of the chamber for most of the measurements and is moved higher in the chamber toward the end of the study.

The procedure for generating ice crystals in the DCC is to moisten and seed the chamber with cloud condensation nuclei (CCN), to cool and lower the pressure in the chamber until a water cloud forms, and to keep cooling until a desired temperature is reached when ice nuclei (IN) are injected and ice nucleation occurs (DeMott and Rogers 1990; DeMott 1995). The air in the chamber is gently stirred so that nucleation occurs rapidly throughout and exposes the FSSP, 1D, and PVM to ice crystals.

An experiment (experiment 5) with outputs similar to those of the other experiments run in the DCC is illustrated in Fig. 1 with the time dependence of pressure (Fig. 1a), temperature (Fig. 1b), moisture (Fig. 1c), and FSSP (Figs. 1d–f) and 1D measurements (Figs. 1g,h). [Droplet coincidence losses for the FSSP concentration in Fig. 1d are not predicted given the means of exposing the droplet stream to the FSSP laser volume (see DeMott and Rogers 1990)]. The total liquid water and ice content (FLWC) calculated on the basis of spherical particles by the FSSP is the dotted data in Fig. 1f. FLWC in Fig. 1f (solid lines) is an estimate of FLWC determined from the heated General Electric (GE) dewpoint hygrometer. The temperature plot (Fig. 1b) has three curves, with the slightly warmer temperature corresponding to the

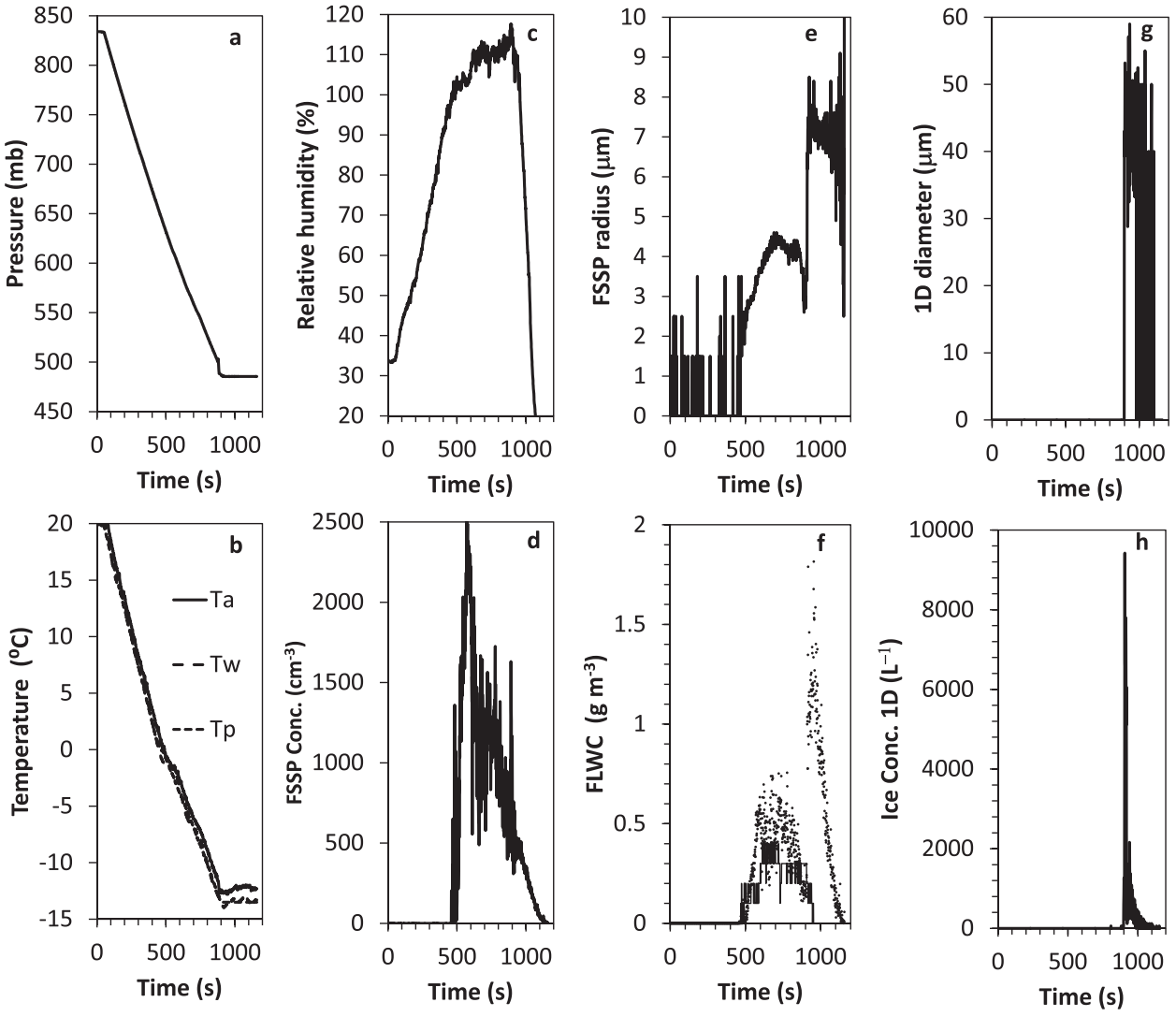

FIG. 1. (a) Pressure, (b) temperature (Ta = air, Tw = wall; Tp = program), and (c) RH in the CSU DCC, and (d)–(f) FSSP and (g),(h) 230-X (1D) data as a function of time during the run of expt 5. In (f), FSSP data (FLWC) are dots; line is water concentration measured by the heated hygrometer. The supersaturated water cloud glaciates at time ~920 s. See text for details. The figure is reproduced from G95.

air temperature in the DCC and the other two temperatures corresponding to the DCC wall and programmed temperatures. The relative humidity in Fig. 1c is from the EG&G dewpoint hygrometer. Both hygrometers are located in the same inlet to the DCC. During experiment 5, droplet condensation occurred at ~480 s, AgI ice nuclei were injected into the DCC at ~900 s, and cloud glaciation followed shortly thereafter as Fig. 1 illustrates.

b. FSSP and PVM

The calculations given in the next section for correction factors for ice-crystal volume V and Re depend on the assumption that the light scattered by the particles in the FSSP and PVM consists of only diffracted light. This assumption may have merit, because both instruments may fall into the class of instruments named "laser diffraction instruments," where a collimated light beam scatters light from particles into a narrow forward angular range. If the particles' dimension is much greater than the wavelength of the incident radiation, then the light scattered in the near-forward direction is dominated by light diffracted by the particles. Evidence exists that this scattered light is proportional to the projected area of the particles for both spherical- and irregular-shaped particles (Van De Hulst 1962; Hodkinson 1966).

The angular range of light scattered in the forward direction by the FSSP is 3.5°–12° (Wendisch and Brenguier 2013). We know from Mie theory that for large nonabsorbing particles about half of the scattered light is caused by diffraction, while the rest is caused by refraction

and reflection. Using phase functions for a variety of ice-crystal habits calculated by Takano and Liou (1989, 1995) and Liou (1992), Gerber et al. (2000) showed that about half of the total scattered light occurs at forward-scattering angles <2°, consistent with the predominance of diffracted light. The FSSP is also somewhat sensitive to the refractive index of the particles (see, e.g., Gayet et al. 1996). These factors suggest that the FSSP may not accurately produce the particles' projected area as required by diffracted-only scattered light, because it must also include some light scattered by refraction through the particles and thus be affected by particle shape. Thus, the question arises, to what degree can the FSSP be considered a laser diffraction instrument that gives useable values for the particles' projected area? Relating the FSSP outputs to the DCC ice crystals can address this question.

The angular range of the scattered light in the PVM is 0.2°–6°, so that light diffracted by the particles dominates. However, given the geometry of the light beam and the irradiated volume in the PVM, the scattered light must be weighted as a function of the scattering angle, which leads to some uncertainty in producing an output proportional to the projected area of the particles.

3. V and Re correction factors

Much has been published on parameterizing ice-crystal properties such mass m, Re, terminal velocity V_t, projected area A_p, and effective density ρ_e for ice particles covering a large range in size and geometry; see, for example, studies by Mason (1957), Locatelli and Hobbs (1974), Mitchell (1996), Heymsfield et al. (2002, 2004, 2007a,b, 2010), Heymsfield (2007), Heymsfield and Miloshevich (2003), and Schmitt and Heymsfield (2007). These studies are based on assigning the maximum dimension D of the ice-crystal projected area as the diameter of the circle circumscribing the crystal, and then using power-law relationships with coefficients to establish formulas for other ice-crystal properties.

The present study is limited to a set of ideal ice crystals used by Takano and Liou (1995) to calculate the crystals' ice volume, and projected area termed G by Takano and Liou for crystals randomly oriented in space. The set of ice crystals includes plates, columns, capped columns, rosettes, and dendrites; see Fig. 2. The values of V and G given by Takano and Liou (1995) provide the basis for calculating corrections for V and Re measured by the FSSP and the PVM for such crystals. Contrary to the earlier studies, this approach does not use D of the circle circumscribed around the crystals. Randomly oriented prolate and oblate spheroidal ice-crystal types (not shown) are also used in the present study.

The corrections for V and Re for aspheric ice crystals are related to the following equations for IWC, PSA, and Re for spherical ice crystals:

$$\mathrm{IWC} = \frac{4\pi\rho_i}{3}\sum_r r^3 n(r), \tag{1}$$

$$\mathrm{PSA} = 4\pi\sum_r r^2 n(r), \quad \text{and} \tag{2}$$

$$\mathrm{Re} = \frac{3}{\rho_i}\frac{\mathrm{IWC}}{\mathrm{PSA}}, \tag{3}$$

where $\rho_i = 0.917\,\mathrm{g\,cm^{-3}}$ is the density of ice and $n(r)$ is the size distribution of the ice crystals.

For the simplest form of ice crystal shown in the Fig. 2, the solid hexagonal crystal without end cavities, Takano and Liou (1995) give

$$G = 3a^2\left[\sqrt{3} + 4(c/2a)\right]/4 \tag{4}$$

as the calculated projected area of randomly oriented crystals, where c is the length (or thickness) of the crystal and $2a$ is the maximum width.

If the FSSP and PVM operate as diffraction-only instruments, then the application of Eq. (3) to ice crystals needs modification of both PSA and IWC. PSA in Eq. (3) can use Eq. (4) since G = PSA/4 for randomly oriented convex particles (Van De Hulst 1962), such as hexagonal plate and columnar ice crystals (Takano and Liou 1995). In Eq. (3), IWC must be replaced by an ice volume V_d calculated for a spherical particle with the same projected area as G. Using the radius, surface area (PSA/4), and volume of this sphere permits the calculation of V_d in terms of G:

$$V_d = 4\pi^{-1/2}G^{3/2}/3, \tag{5}$$

which is termed the diffraction volume. This is larger than the actual V of the hexagonal ice crystal given by Takano and Liou (1995) as

$$V = 3\sqrt{3}a^2c/2. \tag{6}$$

The ratio of V/V_d is given by

$$C_f = \frac{V}{V_d} = \frac{3\sqrt{\pi}(c/a)}{\left[\sqrt{3} + 2(c/a)\right]^{3/2}}, \tag{7}$$

termed the correction factor for V that must be applied to Eq. (1) as well as to the numerator of Eq. (3) so that Eq. (1) for a single crystal of given size and shape becomes

$$\mathrm{IWC} = \rho_i V_d C_f \tag{8}$$

and Eq. (3) becomes

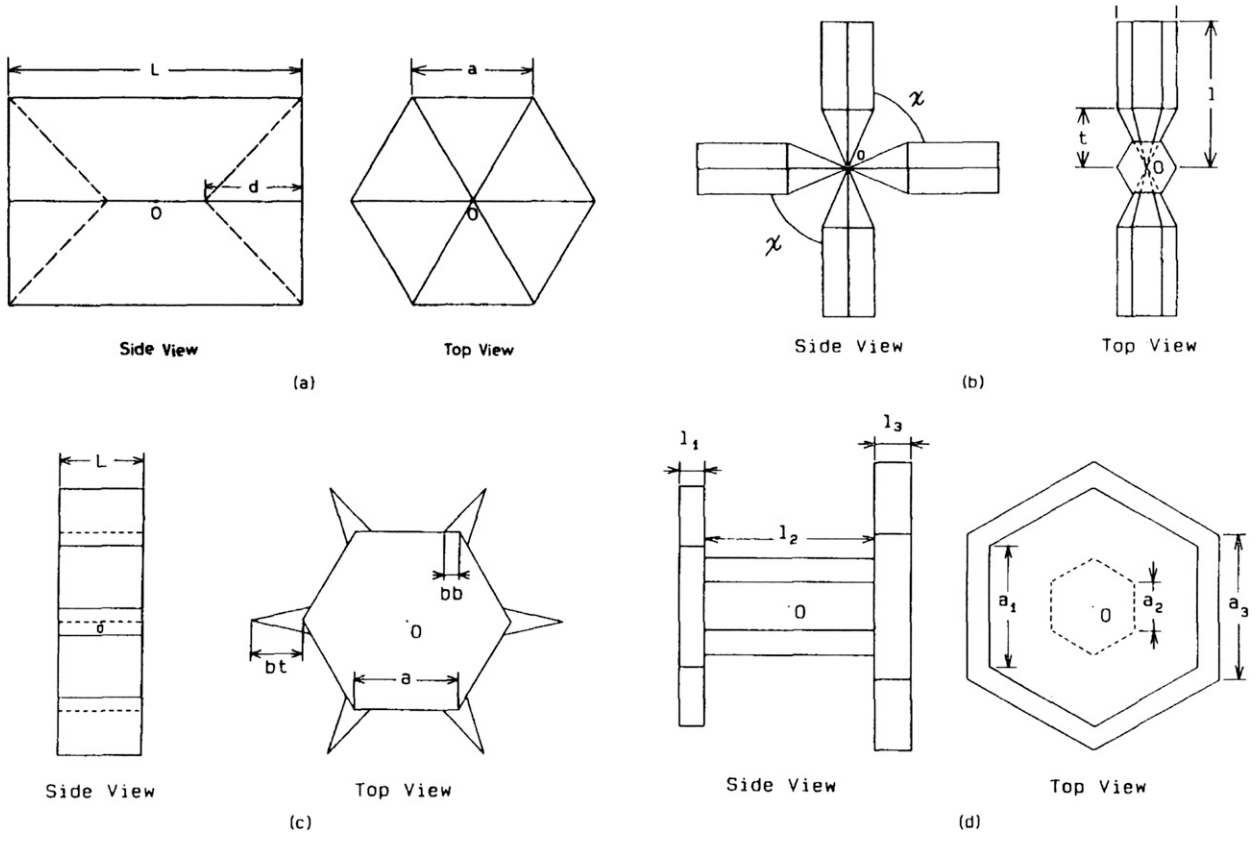

FIG. 2. Model geometry for (a) hollow column, (b) bullet rosette, (c) dendrite, and (d) capped column [reproduced with permission from Takano and Liou (1995)]. The lengths L and l in this plot are changed to the symbol c in the present analysis, and the width $2a$ of the crystals remains the same. The label bb is dendrite branch width and bt is branch length. The mean crossing angle $\chi = 70°$ between the arms of the bullet rosette (see Takano and Liou).

$$\mathrm{Re} = \frac{3V_d C_f}{4G}, \tag{9}$$

which is equivalent to Re given by Foot (1988), except for the correction in the numerator for ice-crystal volume based on ice-crystal habit.

Figure 3 shows the resulting C_f values as a function of c/a calculated using Eq. (7) for the solid hexagonal plate and the columnar ice crystals. Also shown are C_f values calculated for the other crystals in Fig. 2, including hollow columns, solid rosettes, solid dendrites, and solid capped columns. The value of V in Eq. (7) is again given by Takano and Liou (1995), but V_d differs from Eq. (5) for the other crystals because they are no longer convex. Concave crystals require a "shadowing factor" s (Takano and Liou 1995) so that $G = s\mathrm{PSA}/4$, which leads to including the factor $s^{2/3}$ in the denominator of Eq. (5). In Eq. (9), Re is also changed with s included in the numerator. Takano and Liou (1995) provide values for s for different concave crystals. They provide an analytical expression for s for hollow columns, and a limited number of numerical values are provided for the remaining crystals. For the present calculation, $s = 0.94$ is used for solid rosettes, $s = 0.87$ is used for solid capped columns, and s values are interpolated between values given by Takano and Liou (1995) for solid dendrites and over a range of bt/a chosen for Fig. 3. The volume corrections in Fig. 3 are reduced (C_f is larger) by a relatively small amount if s is included. Figure 3 also includes C_f values for solid prolate and oblate spheroids described by Tee (2005).

The Takano and Liou (1995) modeled ice-crystal geometries shown in Fig. 2 have details that are not all represented by curves in Fig. 3. Instead, choices are made for a limited set of details, listed in Table 1, resulting in the given C_f curves in Fig. 3. No attempt is made here to pick details representative of the actual geometric range of small ambient ice crystals. Other choices include using $t = c/2$ for the rosette curves, and applying the factor $(1 - 2d/3c)$ used for hollow columns also to the C_f equation for solid rosettes to generate the two curves for hollow rosettes where $d/c = 0.2$ and $d/c = 0.4$. The filled and open circular data points are measurements discussed in the next section.

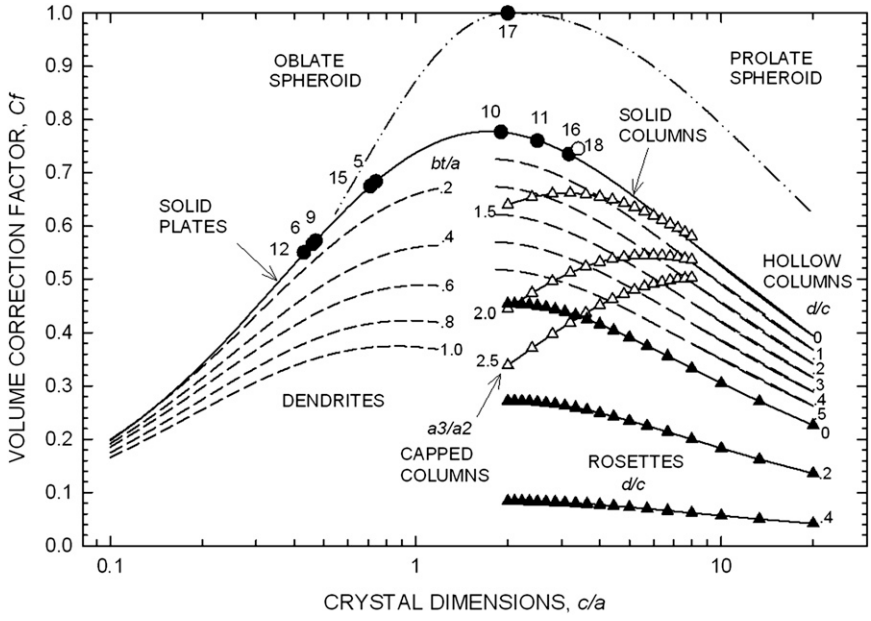

FIG. 3. The ice-crystal volume C_f for PVM and FSSP calculated for the ice-crystal habits shown in Fig. 2 and for spheroids as a function of the ice-crystal dimensions, where c is the crystal length (or thickness) and a is one-half the crystal width. The data consisting of circles are explained in the text.

4. DCC measurements

Eighteen experiments were run in the DCC, 10 of which included detailed ice-crystal analysis; see Table 2 for a brief description of the 10 experiments (all 18 experiments are described in detail in G95). Table 2 shows that during each experiment, one or more 60-s intervals were used for detailed ice-crystal analysis, and it shows

TABLE 1. Ice-crystal habits, equations for crystal volume correction factor C_f, Takano and Liou text and equations, where square brackets [ ] denote TK equation numbers for the volume of the crystals V and their projected area G assuming random crystal orientation, and for Tee equations, which are represented by curly braces { }, for the area A and G of the spheroids Variables under the C_f column are defined and illustrated in Fig. 1.

Crystal type	V, A	G	C_f
Solid hexagonal plates and columns	[TK]	[TK]	$\dfrac{3\sqrt{\pi}(c/a)}{\left[\sqrt{3}+2(c/a)\right]^{3/2}}$
Hollow columns	[(6a)]	[(6b)]	$C_f(\text{solid hex}) \times \left(1-\dfrac{2d}{3c}\right)$
Rosette	[(12a)]	[(12b)]	$\dfrac{2\sqrt{2\pi(a/c)}}{\left[\sqrt{3}(a/c)+2+\sqrt{3(a/c)^2+2}\right]^{3/2}}$
Dendrite	[(14a)]	[(14b)]	$a = 40$ Eq. (5) bb = 8 bt = 8, 16, 24, 32, 40 $c/a = l_2/a_3$
Capped column	[(15a)]	[(15b)]	$a_1 = 0.8a_3$ $\quad l_1 = l_2/7$ Eq. (5) $a_2 = 10, 12.5, 16.7$ $\quad l_2 = c$ $a_3 = 25$ $\quad l_3 = 3l_2/14$
Prolate spheroid	{(3)}	{(3)}/4	$\dfrac{2c\sqrt{a/2}}{\left(\dfrac{c\arcsin\sqrt{q}}{2\sqrt{q}}+a\right)^{3/2}}; \quad q = 1-\dfrac{4a^2}{c^2}$
Oblate spheroid	{(3)}	{(3)}/4	$\dfrac{4b\sqrt{c/2}}{\left(\dfrac{b\arcsin\ h\sqrt{-q}}{\sqrt{-q}}+c/2\right)}$

TABLE 2. Experiments run in the CSU DCC used in the present analysis. During each experiment one or more intervals lasting 60 s were used for detailed crystal analysis.

Expt No.	Interval No.	Description
5	1, 2, 3	Hex plates with some dendritic structure to about 60-μm diameter, −10°C
6	4	Hex plates to about 150 μm, −10°C
9	5, 6	Hex plates to about 50 μm, −18°C; add aspirator to base of PVM
10	7	Columns to about 50 μm, −6°C
11	8, 9	Mostly hex plates to <20 μm, −23.5°C
12	10, 11	Hex plates with dendritic features to 100 μm, −15.5°C
15	12	Hex plates to 80 μm, −12°C; move PVM toward center of DCC
16	13	Columns to 40 μm, −7°C
17	14, 15	Spherical polycrystals to about 10 μm, −30°C
18	16, 17, 18	Mostly columns, −33°C

that crystal habits were primarily hexagonal plates and columns. Two experiments (5 and 12) showed plates with dendritic features, and experiment 17 showed small and nearly spherical crystals. The film loop camera was sufficient to permit manual evaluation of c and a ice-crystal dimensions; however, the camera's limited resolution (5–10 μm per pixel) prevented establishing additional details for crystals with dendritic features. The average c and a data for each experiment, except for experiments 17 and 18, are used to locate in Fig. 3 the value of C_f (solid circles) on the C_f curve given by Eq. (7). The data point for experiment 17 is located at $C_f = 1.0$ given the observed quasi-spherical particles so that $c = \sim 2a$, and the data point for experiment 18 (hollow circle) is established by a direct estimate of V/V_d described in the following.

The individual instruments in the DCC were judged to be unable to directly determine the parameters LWC, PSA, Re, and the size distribution of the crystals for permitting comparisons between the PVM and FSSP. For that reason, the following procedure is used to produce reference values (TOT) of the parameters to which the parameters measured by the PVM and FSSP are compared. The crystals deposited on the video film loop are manually evaluated for habit, dimensions, and relative size distribution. The crystal concentrations measured by the FSSP and the 1D are then applied to the relative size distribution of the crystals on the film loop to produce the reference number size distributions. By applying the Redder and Fukuta (1989) empirical algorithms relating ice-crystal dimensions and crystal mass for plates and columns, IWC is calculated to produce the reference IWC size distributions. (Two experiments—11 and 17—directly used the FSSP spectra to calculate IWC instead of using the Redder–Fukuta approach, because the crystals were small and nearly isometric.) By applying 4G to the reference number size distributions, PSA is calculated. These IWC and PSA values are the reference values termed TOTWC and TOTPSA, respectively, to which the uncorrected and corrected FSSP and PVM measurements are compared in the following. (The WC in TOTWC and PVMWC refers to "water content" composed of the sum of LWC and IWC present in the clouds. In all but one of the intervals listed in Table 2, LWC is negligible so that PVM IWC = PVMWC. There is a presence of LWC at the beginning of interval 1 of experiment 5.) The reference Re (TOTREFF) is given by the ratio of TOTWC/TOTPSA applied to Eq. (3).

The data in Fig. 4 is for experiment 5, and is a typical example showing IWC measurements comparing the Redder–Fukuta approach (TOTWC) with PVMWC. The figure shows that about 200 s elapse until nucleation, sedimentation, and dilution in the chamber reduce ice-crystal concentrations to low values. The figure also shows that the Redder–Fukuta approach produces IWC (TOTWC) much larger than IWC (PVMWC and PVMWC5s) measured by the PVM, which is a result shared by nearly all other experiments in the DCC. Two reasons for this difference appear to be the limited size range of the PVM, which is insufficient for sensing the larger crystals, and the presence of the PVM in the DCC causing ice-crystal evaporation as a result of heat conduction from the probe.

Contrary to the differences between the PVM and FSSP measurements in the DCC for most experiments, two experiments—17 and 18—showed good agreement for LWC, PSA, and Re measurements. In both cases this result is likely due to the small size of the ice crystals that fell within the particle size range measurable by both probes, and because the PVM was moved upward toward the center of the DCC, where its heat output appeared to have less effect. Figure 5 illustrates the PVM–FSSP comparison for IWC and PSA, and shows the FSSP and the1D ice-crystal size distributions for experiment 17. The Redder–Fukuta approach is not used for experiment 17 because of the quasi-spherical shape of the ice crystals. Instead, the FSSP spectra are used directly to calculate IWC and PSA for the two intervals (1 and 15). The good agreement between PVM and FSSP

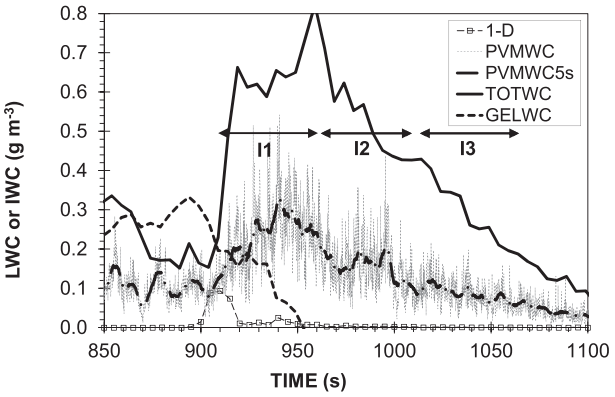

FIG. 4. Comparison of the reference TOTWC calculated during expt 5 to PVM measurements given by PVMWC, 1-Hz data and PVMWC5s, 5-s-average data. PVM measurements strongly underestimate TOTWC. Detailed ice-crystal analysis is done for intervals 1–3. TOTWC is calculated by combining measurements of ice-crystal dimensions and FSSP and 1D spectra, and applying the Redder–Fukuta algorithm (see text). LWC observed by the heated GE hygrometer is given by GELWC. Large ice crystals are observed by the 1D probe.

suggests that both probes were calibrated properly, since they responded in like manner to the quasi-spherical ice crystals.

Figure 6 shows similar plots for experiment 18. In this case the PVM data are compared to the reference IWC (TOTWC) established using the Redder–Fukuta approach, and to PSA (TOTPSA) established by combining measured 4G and reference number size distribution. Figure 6a shows PVMWC larger than TOTWC, which is attributed to the expected overestimate of IWC by the PVM because of the columnar shape of the crystals. The average ratio of PVMWC to TOTWC for the three intervals (16, 17, 18) and the measured a and c values provide a direct value of V/V_d, which is shown as the open circle in Fig. 3. The good agreement for PSA between the PVM and TOTPSA suggests that the PVM and FSSP reacted to the light diffracted by these crystals in about the same way.

A final comparison between Re for PVM and FSSP (PVMRe and FSSPRe, respectively) is shown in Fig. 7, where measured Re values (top plot) for all intervals (1–18) of the experiments are compared to the reference TOTREFF based on the Redder–Fukuta approach using measures of the a and c dimensions of solid plates and columns. Figure 7 (top) shows good agreement between PVMRe and TOTREFF. This agreement is judged fortuitous and is thought to be a result of the lack of response of the PVM to larger crystals and its heat release causing crystal evaporation. The FSSPRe data in Fig. 7 (top), determined for Fig. 7 by assuming spherical crystal shape, shows the expected overestimate of TOTREFF

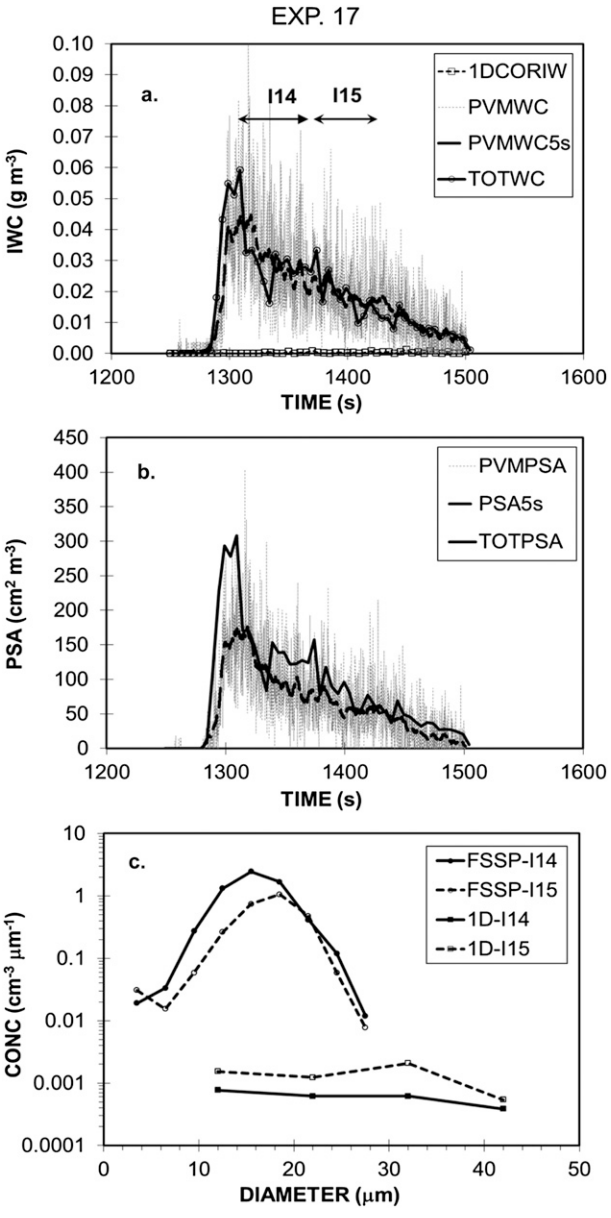

FIG. 5. (a) Comparison of 1-Hz and 5-s-average PVMWC data for quasi-spherical ice crystals for intervals 14 and 15 during expt 17 to reference TOTWC. (b) Comparison of PVMPSA (1-Hz data) to reference TOTPSA. PSA5s is 5-s average PSA data. Comparisons show good agreement. (c) Ice-crystal size spectra measured by the FSSP (top two spectra) and by the 1D (bottom two spectra) for both intervals.

for the nonspherical crystals. Figure 7 (bottom) shows PVMRe and FSSPRe values adjusted by applying the factor C_f, which is proportional to Re according to Eq. (9), and by using measured mean values of a and c for each of the intervals. The FSSPRe values now agree better with TOTREFF, while the PVMRe shows a significant underestimate that reflects the measurement problems of PVM in the DCC.

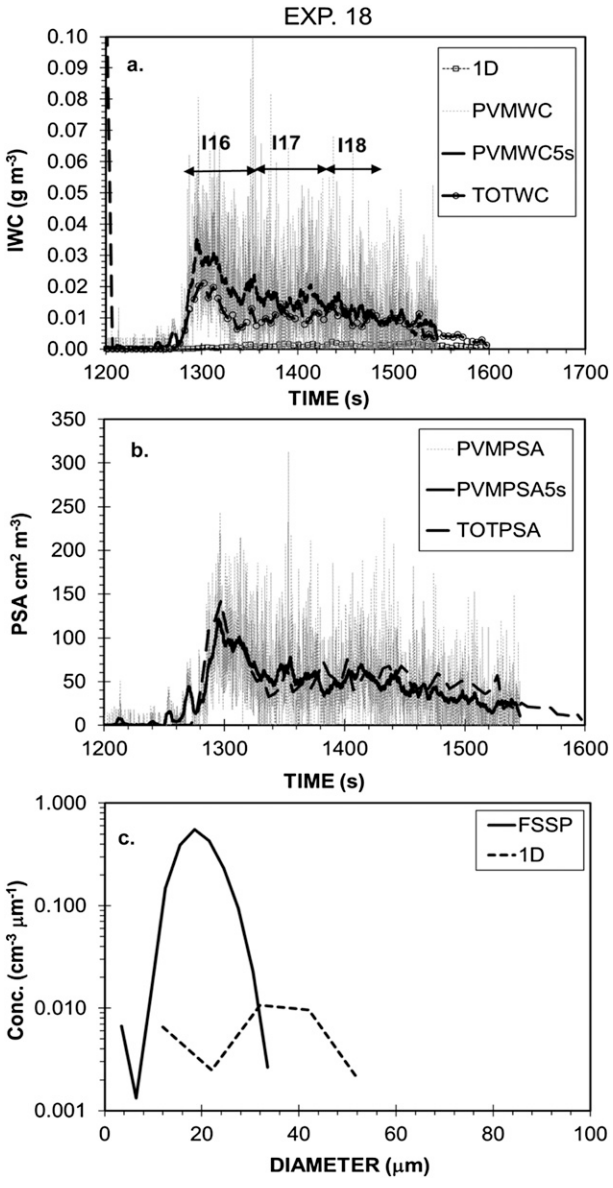

FIG. 6. (a) Comparison of 1-Hz and 5-s-average PVMWC data for expt 18 to reference TOTWC for hexagonal ice crystals; PVMWC overestimates TOTWC. (b) Comparison of PSA to reference TOTPSA (1-Hz data); PVMPSA5s (5-s average data) is the darker curve. (c) Mean FSSP and 1D spectra for the three intervals.

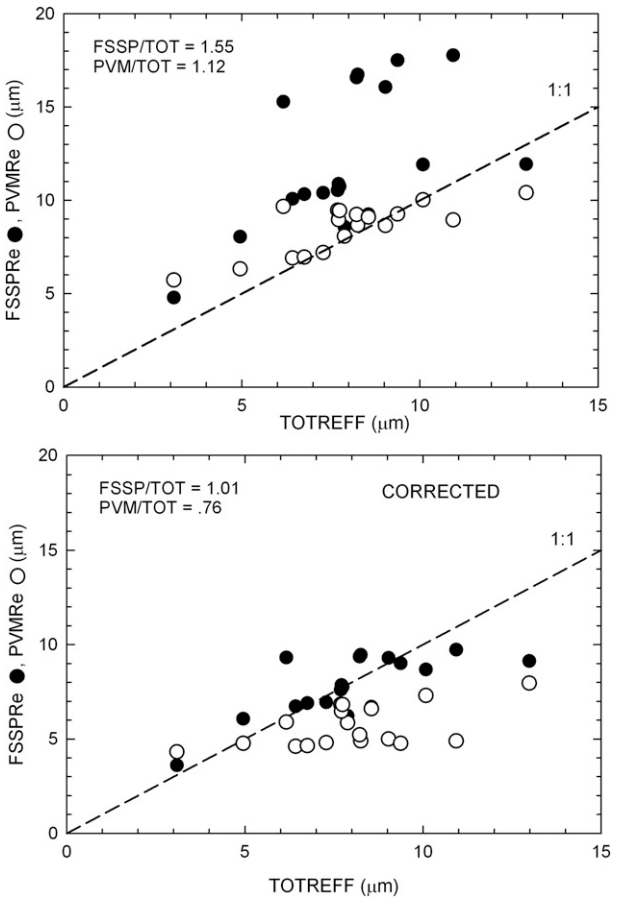

FIG. 7. (top) The mean Re in ice clouds measured by the FSSP and PVM in each interval of the 10 DCC experiments (see Table 2), and (bottom) the same measurements adjusted with the volume C_f as a function of the reference Re given by TOTREFF.

5. Conclusions

The ice-crystal study by G95 was only partially successful in comparing the FSSP and PVM responses to ice crystals generated in the DCC. A significant problem appeared to be heat release from the PVM located inside the DCC during experiments that tended to evaporate ice crystals, causing differences between the FSSP and PVM measurements. Another difficulty was the different size response of the two probes with the PVM LWC channel causing unreliable Re measurements for particle sizes approximately greater than 25-μm diameter. The FSSP measured Re to 45-μm diameter. Also, the PVM does not have a sharp size cutoff unlike the FSSP for large particle sizes, further complicating comparisons. The potential usefulness of the PVM relates to its sampling volume that is ~50 000 greater than the sampling volume of the FSSP, providing a much smaller statistical sampling error. The PVM used during the DCC experiments had a convergent laser beam that caused the limited size response for the LWC channel. Matching better FSSP and PVM responses requires using a less convergent laser beam in the PVM.

An obvious question is how useful is the C_f data shown in Fig. 3 for small ambient ice crystals? As mentioned, the apparent solution of the ice-crystal shattering effect on probes such as the FSSP makes C_f data potentially useful when small crystals are encountered. However, FSSP and PVM data cannot stand alone if corrections

are to be made, since such data must be used in conjunction with high-resolution imaging probes, such as Cloud Particle Imaging (CPI) and 2D Stereo (2D-S; SPEC Inc.), to provide some information on ice-crystal habit. The usefulness of C_f values in Fig. 3 also depends on the assumption that the ice crystals are randomly oriented, because ambient ice crystals can orient themselves in a nonrandom fashion (see, e.g., Platt et al. 1978; Klett 1995; Zhou et al. 2012). An additional possibility is that distortion of streamlines associated with the use of these probes during aircraft flight could alter ambient ice-crystal orientation.

A further complication in using the C_f data is the complexity of small ambient ice crystals that can be much greater than the ideal ice-crystal habits dealt with in this study; see, for example, the coagulated small ice crystals described by Schmitt and Heymsfield (2010). Another example is the rosettes described by Heymsfield et al. (2002) that can have many more arms and complexity than the four-arm rosette model used for the curves in Fig. 3. However, rosettes with maximum dimensions $<50\,\mu$m appear to be rare in imaging data, so that the rosette curves in Fig. 3 may apply more to larger rosettes.

The limited number of comparisons of IWC, PSA, and Re between FSSP and PVM measurements in the DCC that show good agreement are for hexagonal ice crystals with smaller sizes and when the heating effect from the PVM in the DCC is less. These results suggest that the application of C_f for IWC and Re measurements by both probes may be useful in adjusting such measurements given the above-mentioned caveats. Both probes behave approximately as ''laser diffraction instruments''; deviation from this behavior by the FSSP could not be determined because of the resolution of the present measurements.

Small ambient ice crystals are important optically, especially at higher altitude (see, e.g., Heymsfield and Miloshevich 2003), and they need to be measured accurately. Additional chamber studies of ice crystals with habits different from those dealt with here are also desirable.

Acknowledgments. The present analysis was supported by NASA Goddard Grant NNX11AB67G. Thanks are also due to David Rogers, who participated in this study.

REFERENCES

Baumgardner, D., and Coauthors, 2011: Airborne instruments to measure atmospheric aerosol particles, clouds and radiation: A cook's tour of mature and emerging technology. *Atmos. Res.,* **102,** 10–29, doi:10.1016/j.atmosres.2011.06.021.

Borrmann, S. A., B. Luo, and M. Mishenko, 2000: Application of the **T**-matrix method to the measurement of aspheric (ellipsoidal) particles with forward scattering optical particle counters. *J. Aerosol Sci.,* **31,** 789–799, doi:10.1016/S0021-8502(99)00563-7.

DeMott, P. J., 1988: Comparison of the behavior of AgI-type ice nucleating aerosols in the laboratory-simulated clouds. *J. Wea. Modif.,* **20,** 444–450.

——, 1990: An exploratory study of ice nucleation by soot aerosols. *J. Appl. Meteor.,* **29,** 1072–1079, doi:10.1175/1520-0450(1990)029<1072:AESOIN>2.0.CO;2.

——, 1995: Quantitative descriptions of ice formation mechanisms of silver iodide-type aerosols. *Atmos. Res.,* **38,** 63–99, doi:10.1016/0169-8095(94)00088-U.

——, and D. C. Rogers, 1990: Freezing nucleation rates of dilute solution droplets measured between −30°C and −40°C in laboratory simulations of natural clouds. *J. Atmos. Sci.,* **47,** 1056–1064, doi:10.1175/1520-0469(1990)047<1056:FNRODS>2.0.CO;2.

Febvre, G., J.-F. Gayet, V. Shcherbakov, C. Gourbeyre, and O. Jourdan, 2012: Effects of ice crystals on the FSSP measurements in mixed phase clouds. *Atmos. Chem. Phys. Discuss.,* **12,** 7909–7947, doi:10.5194/acpd-12-7909-2012.

Foot, J. S., 1988: Some observations of the optical properties of clouds. *Quart. J. Roy. Meteor. Soc.,* **114,** 145–164, doi:10.1002/qj.49711447908.

Gardiner, B. A., and J. Hallett, 1985: Degradation of in-cloud forward scattering spectrometer probe measurements in the presence of ice particles. *J. Atmos. Oceanic Technol.,* **2,** 171–180, doi:10.1175/1520-0426(1985)002<0171:DOICFS>2.0.CO;2.

Gayet, J.-F., G. Febvre, and H. Larsen, 1996: The reliability of the PMS FSSP in the presence of small ice crystals. *J. Atmos. Oceanic Technol.,* **13,** 1300–1310, doi:10.1175/1520-0426(1996)013<1300:TROTPF>2.0.CO;2.

——, and Coauthors, 2012: The evolution of microphysical and optical properties of an A380 contrail in the vortex phase. *Atmos. Chem. Phys.,* **12,** 6629–6643, doi:10.5194/acp-12-6629-2012.

Gerber, H., P. J. DeMott, and D. C. Rogers, 1995: Laboratory investigation of direct measurement of ice water content, ice surface area, and effective radius of ice crystals using a laser-diffraction instrument. NASA Ames Research Center Tech. Rep. NAS2-1426, 142 pp. [Available online at http://ntrs.nasa.gov/archive/nasa/casi.ntrs.nasa.gov/20000023203.pdf.]

——, C. H. Twohy, B. Gandrud, A. J. Heymsfield, G. M. McFarquhar, P. J. DeMott, and D. C. Rogers, 1998: Measurements of wave-cloud microphysical properties with two new aircraft probes. *Geophys. Res. Lett.,* **25,** 1117–1120, doi:10.1029/97GL03310.

——, Y. Takano, T. J. Garrett, and P. V. Hobbs, 2000: Nephelometer measurements of the asymmetry parameter, volume extinction coefficient, and backscatter ratio in Arctic clouds. *J. Atmos. Sci.,* **57,** 3021–3034, doi:10.1175/1520-0469(2000)057<3021:NMOTAP>2.0.CO;2.

Heymsfield, A. J., 2007: On the measurement of small ice particles in clouds. *Geophys. Res. Lett.,* **34,** doi:10.1029/2007GL030951.

——, and L. M. Miloshevich, 2003: Parameterization for the cross-sectional area and extinction of cirrus and stratiform ice cloud particles. *J. Atmos. Sci.,* **60,** 936–956, doi:10.1175/1520-0469(2003)060<0936:PFTCSA>2.0.CO;2.

——, S. Lewis, A. Bansemer, J. Iaquinta, and L. M. Miloschevich, 2002: A general approach for deriving the properties of cirrus and stratiform ice cloud particles. *J. Atmos. Sci.,* **59,** 3–29, doi:10.1175/1520-0469(2002)059<0003:AGAFDT>2.0.CO;2.

——, A. Bansemer, C. Schmitt, C. H. Twohy, and M. R. Poellot, 2004: Effective ice particle densities derived from aircraft data. *J. Atmos. Sci.,* **61,** 982–1003, doi:10.1175/1520-0469(2004)061<0982:EIPDDF>2.0.CO;2.

——, ——, and C. H. Twohy, 2007a: Refinements of ice particle mass dimensional and terminal velocity relationships for ice clouds. Part I: Temperature dependence. *J. Atmos. Sci.,* **64,** 1047–1067, doi:10.1175/JAS3890.1.

——, G.-J. Van Zadelhoff, D. P. Donovan, F. Fabry, R. J. Hogan, and A. J. Illingsworth, 2007b: Refinements to ice particle mass dimensional and terminal velocity relationships for ice clouds. Part II: Evaluation and parameterization of ensemble ice particle sedimentation velocities. *J. Atmos. Sci.,* **64,** 1068–1088, doi:10.1175/JAS3900.1.

——, C. Schmitt, A. Bansemer, and C. H. Twohy, 2010: Improved representation of ice particle masses based on observations in natural clouds. *J. Atmos. Sci.,* **67,** 3303–3318, doi:10.1175/2010JAS3507.1.

Hodkinson, J. R., 1966: The optical measurement of aerosols. *Aerosol Science,* C. N. Davies, Ed., Academic Press, 287–357.

Jensen, E. J., and Coauthors, 2009: On the importance of small ice crystals in tropical anvil cirrus. *Atmos. Chem. Phys.,* **9,** 5519–5537, doi:10.5194/acp-9-5519-2009.

Klett, J. D., 1995: Orientation model for particles in turbulence. *J. Atmos. Sci.,* **52,** 2276–2285, doi:10.1175/1520-0469(1995)052<2276:OMFPIT>2.0.CO;2.

Korolev, A. V., E. F. Emery, J. W. Strapp, S. G. Cober, G. A. Isaac, M. Wasey, and D. Marcotte, 2011: Small ice particles in tropospheric clouds: Fact of artifact? *Bull. Amer. Meteor. Soc.,* **92,** 967–973, doi:10.1175/2010BAMS3141.1.

——, E. Emery, and K. Creelman, 2013: Modification and tests of particle probe tips to mitigate effects of ice shattering. *J. Atmos. Oceanic Technol.,* **30,** 690–708, doi:10.1175/JTECH-D-12-00142.1.

Liou, K. N., 1992: *Radiation and Cloud Processes in the Atmosphere: Theory, Observations, and Modeling.* Oxford University Press, 487 pp.

Locatelli, J. D., and P. V. Hobbs, 1974: Fall speeds and masses of solid precipitation particles. *J. Geophys. Res.,* **79,** 2185–2197, doi:10.1029/JC079i015p02185.

Mason, B. J., 1957: *The Physics of Clouds.* Oxford University Press, 671 pp.

McFarquhar, G. M., J. Um, M. Freer, D. Baumgardner, and G. L. Kok, 2007: Importance of small ice crystals to cirrus properties: Observations from the Tropical Warm Pool International Cloud Experiment (TWP-ICE). *Geophys. Res. Lett.,* **34,** L13803, doi:10.1029/2007GL029865.

Mitchell, D. L., 1996: Use of mass- and area-dimensional power laws for determining precipitation particle terminal velocities. *J. Atmos. Sci.,* **53,** 1710–1723, doi:10.1175/1520-0469(1996)053<1710:UOMAAD>2.0.CO;2.

Platt, C. M. R., N. L. Abshire, and G. T. McNice, 1978: Some microphysical properties of an ice cloud from lidar observations of horizontally oriented crystals. *J. Appl. Meteor.,* **17,** 1220–1224, doi:10.1175/1520-0450(1978)017<1220:SMPOAI>2.0.CO;2.

Redder, C. R., and N. Fukuta, 1989: Empirical equations of ice crystal growth microphysics for modeling and analysis, I. Mass and dimensions. *Atmos. Res.,* **24,** 247–272, doi:10.1016/0169-8095(89)90048-3.

Schmitt, C. G., and A. J. Heymsfield, 2007: On the occurrence of hollow bullet rosette- and column-shaped ice crystals in midlatitude cirrus. *J. Atmos. Sci.,* **64,** 4514–4519, doi:10.1175/2007JAS2317.1.

——, and ——, 2010: The dimensional characteristics of ice crystal aggregates from fractal geometry. *J. Atmos. Sci.,* **67,** 1605–1616, doi:10.1175/2009JAS3187.1.

Takano, Y., and K. N. Liou, 1989: Solar radiative transfer in cirrus clouds. Part I: Single-scattering and optical properties of hexagonal ice crystals. *J. Atmos. Sci.,* **46,** 3–19, doi:10.1175/1520-0469(1989)046<0003:SRTICC>2.0.CO;2.

——, and ——, 1995: Radiative transfer in cirrus clouds. Part III: Light scattering by irregular ice crystals. *J. Atmos. Sci.,* **52,** 818–837, doi:10.1175/1520-0469(1995)052<0818:RTICCP>2.0.CO;2.

Tee, G. J., 2005: Surface area and capacity of ellipsoids in *n* dimensions. *N. Z. J. Math.,* **34,** 165–198.

Van De Hulst, H. C., 1962: *Light Scattering by Small Particles.* John Wiley & Sons, 470 pp.

Wendisch, M., and J.-L. Brenguier, Eds., 2013: *Airborne Measurements for Environmental Research: Methods and Instruments.* Series in Atmospheric Physics and Remote Sensing, Wiley, 641 pp., doi:10.1002/9783527653218.

Young, D. F., P. Minnis, D. Baumgardner, and H. Gerber, 1998: Comparison of in situ and satellite-derived cloud properties during SUCCESS. *Geophys. Res. Lett.,* **25,** 1125–1128, doi:10.1029/98GL00116.

Zhou, C., P. Yang, and A. E. Dessler, 2012: Study of horizontally oriented ice crystals with *CALIPSO* observations and comparison with Monte Carlo radiative transfer simulations. *J. Appl. Meteor. Climatol.,* **51,** 1426–1439, doi:10.1175/JAMC-D-11-0265.1.